Solitary-like waves in a liquid foam microchannel

Yann Bouret, Alexandre Cohen, Nathalie Fraysse, Médéric Argentina, Christophe Raufaste

Solitary-like waves in a liquid foam microchannel

Yann Bouret,[1] Alexandre Cohen,[1] Nathalie Fraysse,[1] Médéric Argentina,[2,3] and Christophe Raufaste[1,*]

[1] *Université Côte d'Azur, CNRS, LPMC, France*
[2] *Université Côte d'Azur, CNRS, INLN, France*
[3] *Institut Universitaire de France, 75005 Paris, France*

(Dated: August 18, 2016)

Plateau borders are liquid microchannels located at the contact between three bubbles in liquid foams. They are stable, deformable and can be thought of as quasi-1D model systems to study surface waves in fluid dynamics. We show that the burst of a bubble trapped in a PB produces local constrictions which travel along the liquid channel at constant velocity, without significant change in shape. These patterns are reminiscent of the depression solitary waves encountered in nonlinear systems. By coupling flow inertia to capillary stresses, we derive a simple model that admits solitonic solutions, which we characterized numerically and analytically in the limit of small deformation. These solutions capture most of the features observed experimentally.

PACS numbers: 47.57.Bc, 68.03.-g, 47.55.nb

I. INTRODUCTION

The stability of liquid foams significantly depends on the flow properties of the Plateau borders (PBs), which are wall-free liquid microchannels found at the contact between three bubbles [1]. Each Plateau border (PB) is held by three soap films and has the very specific geometry highlighted in Fig. 1: the PB is inscribed in a triangular prism and its cross section can be approximated by the tangential contact of three arcs of circles of identical radius of curvature [2]. At the foam scale, the PBs form an interconnected porous network through which the liquid runs off (see [3, 4] for a review on foam drainage). The flow properties inside a single PB have also been the subject of several studies [5–11]. Structures made of PBs are robust and most of the perturbations - produced for example by adding liquid in excess - relax to recover steady-state Plateau borders of homogeneous radius profile. The dynamics of the flow triggered in each PB results from the coupling between the deformation of the PB, the fluid properties and the stress at the liquid/gas interface [4, 12]. In all the aforementioned studies, the flow was assumed viscous, due to the small radius of the channel (typically 10 to 100 microns) and the small velocities measured (typically millimeters per second or less).

We recently showed that the perturbation brought to a single PB by making a droplet coalesce with it may actually relax rather quickly (typical velocities are 0.1 to 1 meter per second), according to what we proved to be an inertial regime [13, 14]. Under identified experimental conditions [13], the perturbation is dispersed through the formation of structures analogous to hydraulic jumps driven by capillarity instead of gravity [15]. The occurrence and the dynamics of these capillary hydraulic jumps were satisfactorily modeled by assuming an inertia-dominated plug flow in the PB.

* corresponding author: Christophe.Raufaste@unice.fr

The present study differs from the drop-injected experiment in the way we perturb the PB, leading to a drastically different response of the system. Here, a small bubble is brought to the PB, before being burst. Capillary suction triggers a transient flow in the liquid microchannel and the relaxation process develops local constrictions of the PB. Each constriction travels at constant velocity, without significant deformation over a distance that is large compared to the size of the depression zone. These localized-in-space patterns are reminiscent of solitary waves first introduced by Russell [16] and found in numerous non-linear systems [17]. Theory predicts depression solitary waves as well as elevation ones [18]. In addition to the well-known dark solitons in optics, depression solitary waves were reported at the surface of a thin layer of mercury [19] and at the surface of a levitated water cylinder [20]. In this article, we aim at investigating these new structures observed to travel along PBs. We show that they might be identified to depression solitary waves.

The manuscript is organized as follows. We first depict the bubble-burst experiment and report systematic measurements. Then, we introduce a theoretical model which leads to an ordinary differential equation, whose solutions successfully capture the dynamics of the PB radius of curvature.

II. MATERIAL AND METHODS

The setup is similar to the one implemented for the drop-injected experiment (see [14] for details). By dipping a triangular-prism frame into a surfactant solution, we create a few-centimeter-long, horizontal PB held by three soap films (Fig. 1a,b). The initial radius of curvature of the PB is homogeneous and kept constant by continuously injecting liquid into it; its value can be set by tuning the flow rate. We deduce the local radius of curvature of the PB, R, from its apparent thickness, e, easily measurable on the side view (Fig. 2). The cali-

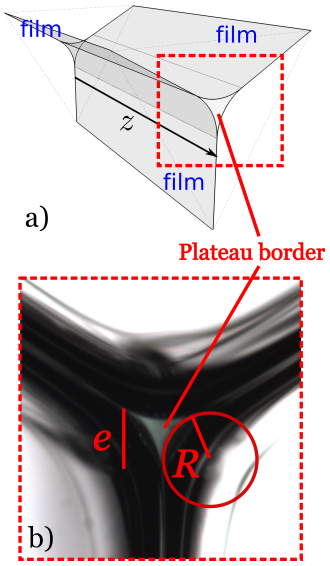

FIG. 1. a) Sketch of the geometry of the Plateau border and its three holding films. b) Cross section of the PB seen through the liquid meniscus formed at the contact with a glass plate.

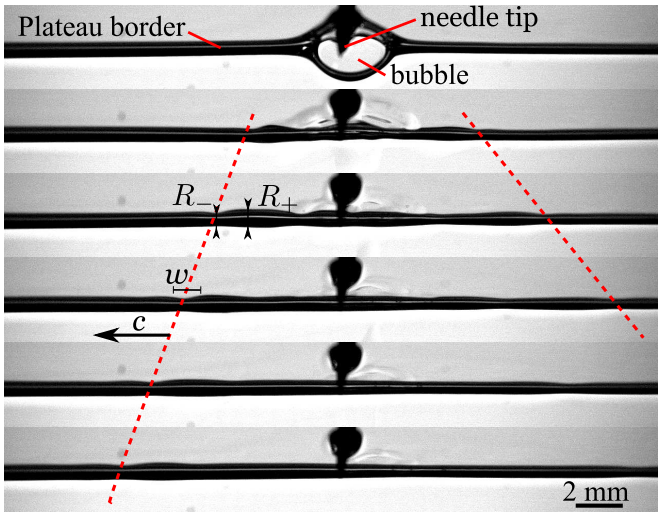

FIG. 2. Image sequence of a typical bubble-burst experiment (small bubble, 10 ms between consecutive images). The bubble can be seen in the first picture; the dark spot which appears above the PB in each of the pictures is the tip of the needle used to burst the bubble. Dashed lines are guides to the eyes to follow the positions of two constrictions visible in the pictures. These constrictions move at constant velocity (0.13 m/s leftward for the constriction on the left, 0.27 m/s rightward for the one on the right). See text for notations.

bration procedure that we perform prior to any experiment (details can be found in [14]) shows that these two quantities are proportional, and that the proportionality constant is very close to 1. For the sake of simplicity, we will hereafter speak of radius of curvature only. The surfactant solution used in the present study was composed

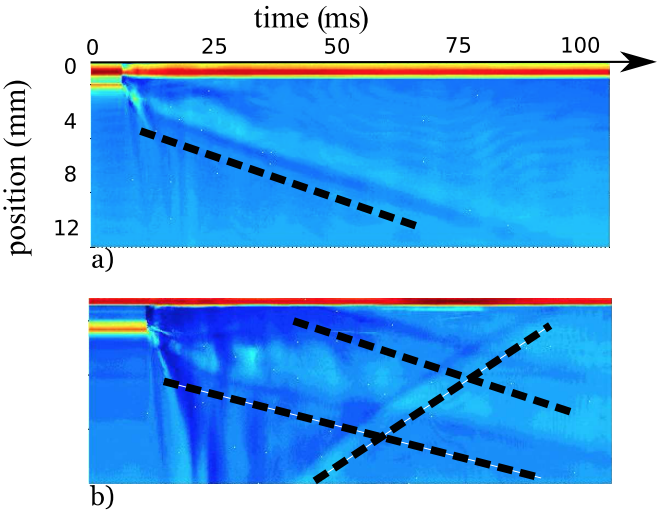

FIG. 3. a) Space-time diagram of the PB radius of curvature built using the left half of the images recorded during the experiment reported in Fig. 2. b) Space-time diagram for an experiment performed with a larger bubble. The red and yellow stripes on top of both diagrams arise from the images of the bubble at short times and of the needle tip at all times. Dark-blue straight stripes reveal constrictions moving along the PB (dashed black lines were plotted slightly offset to emphasize these features).

of TTAB (tetradecyl trimethyl ammonium bromide) dissolved into de-ionized water to a concentration of 3 g/l. It is characterized by tangential stress-free interfaces and the physical properties of this solution are its density $\rho = 1030 \pm 50$ kg.m^{-3}, its surface tension $\gamma = 38 \pm 1$ mN/m and its dynamic viscosity $\eta = 1.04 \pm 0.02$ mPa.s [14].

A bubble, with an initial size small compared to the length of the PB, is gently inserted and held in place into the PB. The tip of a needle pierces the bubble to burst it: this provokes a strong perturbation of the PB at short times. The subsequent relaxation of the PB is recorded with a fast camera at 4000 fps. Fig. 2 displays a set of snapshots that shows the time evolution of the PB. Space-time diagrams of the radius of curvature of the PB are useful to highlight the relaxation dynamics: a color is assigned to the local value of the PB radius of curvature using a color scale that ranges here from dark blue for the thinnest parts of the PB to light blue for the thickest parts. At each time step of a given experiment, the radius profile yields a vertical line of color pixels; the horizontal stack of the columns computed from the whole set of pictures generates the space-time diagram. Two examples of such diagrams are shown in Fig. 3 for two different initial bubble sizes.

III. RESULTS

A few milliseconds after the bubble bursts, the PB radius profile shows constriction zones of small lateral extension, moving apart from the initial bubble location, as evidenced in Fig. 2 and in the movie of the Supplemental Material [21]. Although the variations in radius defining these localized patterns remain small (of the order of ten percent), they can be detected unambiguously and characterized.

Remarkably, the shape of each constriction zone is almost preserved during its propagation along the PB and the constriction remains visible far from the initial bubble position, over distances much larger than its typical size. The minimal radius of curvature of the PB and the width of the depression are denoted R_- and w, respectively. A slight asymmetry in the PB radius of curvature is observed, with a small overshoot at the rear of the constriction. The difference between the PB radius of curvature in front of and behind the constriction is nevertheless very small, of a few percent at most. We note R_+ the radius of curvature of the PB as it overshoots. Ahead of the constriction zone, the deformation of the PB tends to zero, and its radius converges to its initial value. Another noteworthy feature of the localized depression patterns is that they travel along the PB at constant velocity, noted c. All these characteristics appear straightforwardly by considering space-time diagrams. The example of Fig. 3a shows a dark-blue, straight stripe that reveals a thinner, narrow zone of the PB, which travels at constant speed, over more than 10 mm in distance. The lighter stripe adjacent to the previous one stands for the overshoot of the PB radius at the rear of the constriction.

The size of the initial bubble does not significantly affect the constriction shape and dynamics. An increase in the bubble size may only increase the number of constrictions that are created. On the space-time diagram of Fig. 3b, which was obtained after the burst of a large bubble, two constrictions traveling in the same direction, away from the bubble location, are discernible on one half of the PB. Note that a third constriction is also noticeable, going in the reverse direction, as the result of the reflection of some perturbation on the vertex. Interestingly, when this third constriction collides with one of the two others, they cross each other without any significant change in velocity and nor in shape.

Measurements of R_-, R_+, w and c were performed on 41 constriction waves, for various values of the initial radius of curvature of the PB and of the bubble size. R_-, w and c are plotted as a function of the radius R_+ in Fig. 4a, b, and c, respectively. R_- and w appear to be proportional to R_+ (Fig. 4a and b), while c decreases with R_+ (Fig. 4c). Linear fits for R_- and w give: $R_- = (0.80 \pm 0.15)R_+$ and $w = (1.10 \pm 0.15)R_+$.

An estimation of the Reynolds number around 100 is found given typical values of $c \sim 0.2$ m/s and $R_+ \sim 0.5$ mm. This shows that the physics is controlled by a balance between inertia and capillary forces, like in the

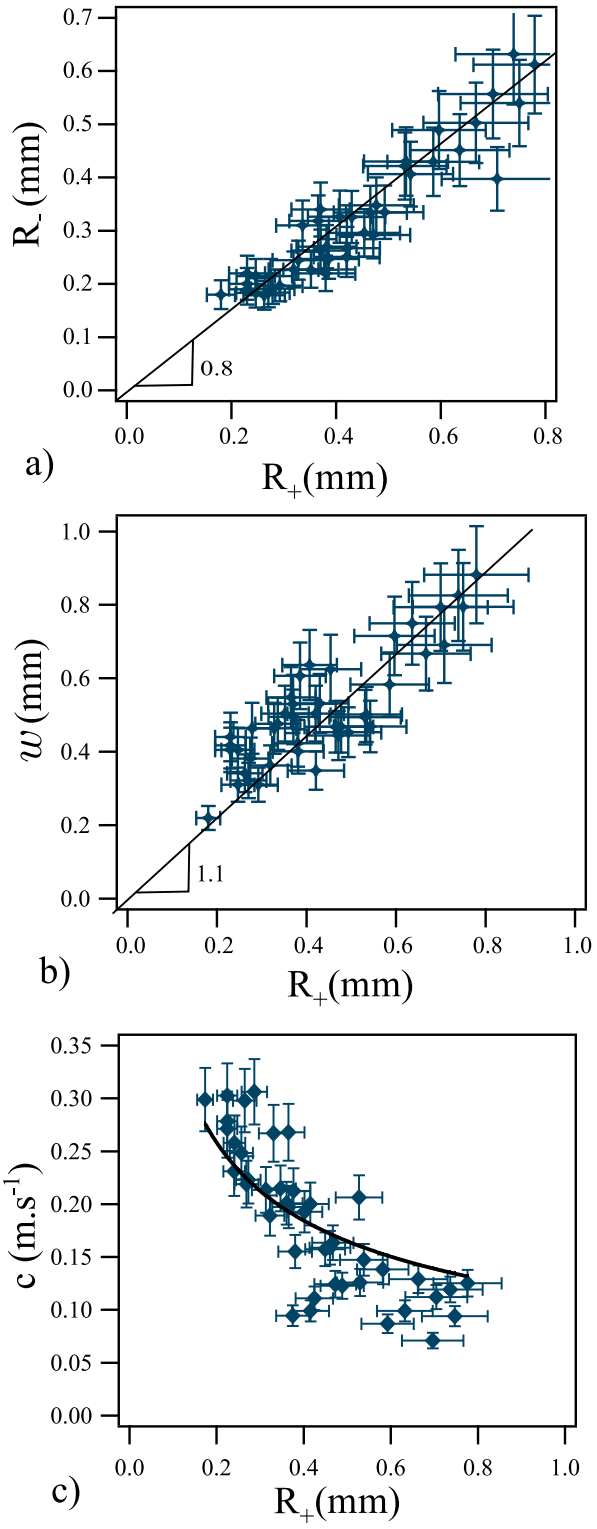

FIG. 4. Geometry and velocity dependence of the constrictions with respect to R_+. a) Amplitude of the constrictions R_-. b) Width of the constrictions w. c) Velocity of the constrictions c. The black lines correspond to the adjustment of the data as stated in the text.

drop-injected experiment [13]. We thus introduce the capillary-inertial velocity $c_0 = \sqrt{\gamma/\rho R_+}$.

Given the experimental dispersion, the data on the velocity c scale reasonably well with the $R_+^{-0.5}$ dependence expected from c_0: the black line in Fig. 4c corresponds to the best fit by a power-law of exponent -0.5. The adjustment leads to

$$c_{\rm exp} = (0.61 \pm 0.12)c_0. \tag{1}$$

The capillary hydraulic jumps observed in the drop-injected experiment are characterized by a velocity proportional to c_0 as well [13, 14]. The prefactor is equal to 1.07, which is roughly twice the one obtained for the depression waves in the bubble-burst experiment. However, it is important to note that hydraulic jumps and depression waves are two different kinds of responses of the PB to a perturbation. Both their geometry and dynamics are different. A capillary hydraulic jump separates two extended regions of distinct, uniform radii of curvature. In that sense it can be regarded as a positive and extended perturbation that requires a significant mass of liquid to be added to the PB to occur. Conversely, depression waves are localized and negative perturbations to an otherwise uniform PB. They do not need an excess of mass to appear. We have observed them in the bubble-burst experiment but they could appear in other situations, including in the drop-injected experiment. However, because their amplitude and velocity are small, the presence of hydraulic jumps are likely to hide them.

IV. MODEL

As for capillary hydraulic jumps, the observations of localized depression patterns traveling at constant velocity along the PB call for a capillary-inertial description of the underlying flow. Assuming that the PB profile and the flow are steady in a reference frame moving with velocity c, Argentina et al. [15] wrote the mass and horizontal momentum balance equations as:

$$\partial_Z \left(uR^2\right) = 0 \tag{2}$$

$$\rho u^2 + \gamma\left(\frac{1}{R} - \beta_1 \partial_{ZZ} R - \beta_2 \frac{(\partial_Z R)^2}{R}\right) - 3\eta\partial_Z u = \frac{d}{R^2}. \tag{3}$$

ρ, γ and η are the density, the surface tension and the viscosity of the liquid, respectively. The velocity u is assumed uniform on the PB cross section, so that both the radius of curvature R and u are functions only of $Z = z - ct$ which defines the longitudinal distance along the Plateau border in the reference frame moving with velocity c. In Eq. (3), the mean curvature of the liquid-gas interface involves two geometrical prefactors $\beta_1 \sim \beta_2 \sim 0.1$ related to the specific shape of a PB. For the sake of simplicity, we set $\beta_1 = \beta_2 = \beta$. Finally, d is an integration constant fixed by the boundary conditions at infinity. The last term in the l.h.s. of Eq. (3) stands for the viscous shear.

This ODE was able to retrieve the existence of the hydraulic jumps observed in the drop-injected experiment. A quantitative agreement was found with the experimental data, and the theoretical prediction that all velocities should fulfill $c > c_0/\sqrt{2}$ proved to be satisfied. Remarkably, it was found that other solutions, localized in space and traveling at velocities $c < c_0/\sqrt{2}$, could also exist. Their shape was numerically computed and found to be a symmetric constriction [15]. Therefore, these solutions appear as good candidates to explain the observations of the bubble-burst experiment. They obey the boundary conditions:

$$R(\pm\infty) = R_+ \tag{4}$$

$$u(\pm\infty) = -c \tag{5}$$

which fixes $d = \rho(cR_+)^2 + \gamma R_+$. As done in [15], we rewrite the equations in a dimensionless form by choosing the scalings $u = cv$, $Z = R_+ s$ and $R = R_+ a$:

$$v = -\frac{1}{a^2} \tag{6}$$

$$\frac{1}{a^4} - \frac{1+1/We}{a^2} + \frac{1}{We}\left(\frac{1}{a} - \beta\left(\partial_{ss}a + \frac{(\partial_s a)^2}{a}\right)\right) - \frac{1}{Re}\frac{6}{a^3}\partial_s a = 0, \tag{7}$$

where we have introduced the Reynolds number, Re, and the Weber number, We:

$$Re = \frac{\rho c R_+}{\eta}, We = \frac{\rho c^2 R_+}{\gamma} \quad . \tag{8}$$

For large values of the Reynolds number, we omit the last term of Eq. (7). Following [15], the resulting equation multiplied by $a^2\partial_s a$ is integrated once with respect to s:

$$\frac{a(s)^2\left(1 - \beta a'(s)^2\right)}{2We} - \frac{(We+1)a(s)}{We} - \frac{1}{a(s)} = -\frac{1+4We}{2We}. \tag{9}$$

The right-hand side of Eq. (9) is the integration constant imposed by the boundary conditions $a(\pm\infty) = 1$. By setting the local minimum of the constriction at $Z = 0$, we have $a(0) = a_- = R_-/R_+$, and $a'(0) = 0$, from what we deduce the following relation between We and a_-:

$$\frac{a_-^2}{2We} - \frac{(We+1)a_-}{We} - \frac{1}{a_-} = -\frac{1+4We}{2We}, \tag{10}$$

which reduces to $a_- = 2We$. From Eq. (8), the velocity c can thus be expressed as function of the constriction aspect ratio a_-:

$$c = c_0\sqrt{\frac{a_-}{2}} \tag{11}$$

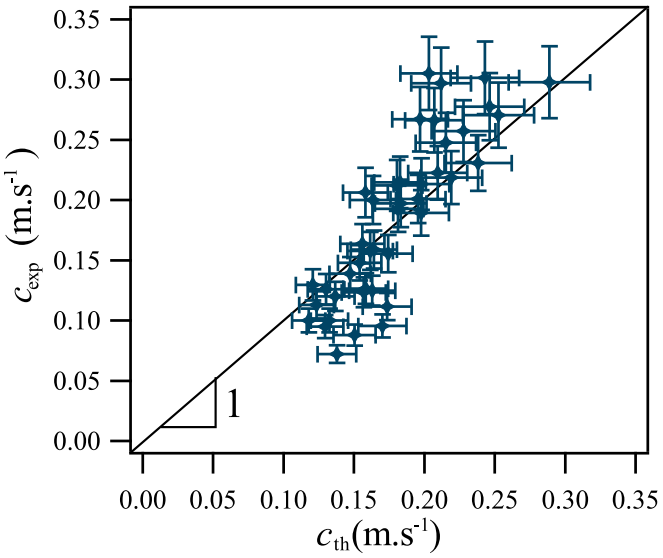

FIG. 5. Measured velocity $c_{\rm exp}$ as a function of the prediction c_{th} for solitary waves of Eq. (11).

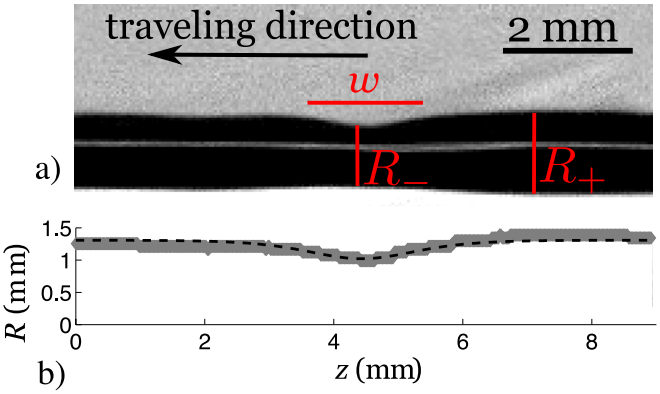

FIG. 6. a) Enlargement of a constriction zone. The width of the constriction w, the radius of the constriction R_- and of the overshoot R_+ are emphasized. b) Radius of curvature profile measured experimentally (light gray) and adjustment by Eq. (14) of the model (dark dashed curve).

As a consequence, since $a_- < 1$, the velocity is bounded: $c < c_0/\sqrt{2}$. This upper limit of the velocity can define the group velocity. For flows with velocity higher than this critical velocity, shock waves are expected to occur and take the form of hydraulic jumps [15]. For their part, the constrictions can be identified to subsonic solitary waves, in a similar way as the surface waves observed for the mercury and levitated water cylinder systems mentioned previously [19, 20].

In Fig. 5, the experimental velocity of each constriction is compared to the velocity predicted by Eq. (11) when using the experimentally measured value for a_-. The agreement is satisfying considering that there is no free parameter. In most of the experimental profiles we measured $a_- \sim 0.8$, such that $c_{th} \sim 0.63 c_0$: the numerical prefactor is very close to the 0.61 value that has been measured experimentally (Eq. (1)).

To proceed further, we compute the radius of curvature profile of a depression solitary wave, analytically to the first order in the limit of small deformations. Eq. (9) can be integrated once with respect to s; we do not report this calculation here neither its weighty resulting expression. From this expression and using perturbation theory, a simple analytical expression for the constriction can be explicitly computed as follows. In the limit of small deformations, we write $a_- = 1 - \varepsilon$, assuming $\varepsilon \ll 1$. By inserting the Ansatz:

$$a = 1 - \varepsilon a_1\left(s\frac{\sqrt{\varepsilon}}{2\sqrt{\beta}}\right) + O\left(\varepsilon^2\right) \qquad (12)$$

into Eq. (9), we obtain

$$\frac{1}{4}\left(\partial_t a_1(t)\right)^2 - a_1(t)^2 + a_1(t)^4 = O(\varepsilon), \qquad (13)$$

where $t = s\frac{\sqrt{\varepsilon}}{2\sqrt{\beta}}$. This equation admits $a_1(t) = 1/\cosh(t)^2$ as a solution. Finally, the profile of the localized structure obeys

$$a(s) = 1 - \frac{(1-a_-)}{\cosh^2\left(s\frac{\sqrt{1-a_-}}{2\sqrt{\beta}}\right)} + O\left((1-a_-)^2\right). \qquad (14)$$

The above formula was tested by looking for the best fit of the experimental profile reported in Fig. 6a with β as a free parameter. The adjustment yields the theoretical profile superposed with the experimental profile in Fig. 6b. The value 0.04 is obtained for β, which is consistent with the expected 0.1 value as mentioned above and in [15].

V. CONCLUSIONS

By means of an experimental study, we have shown that the relaxation dynamics of Plateau borders may exhibit structures having the characteristics of depression solitary waves [18]: these newly observed structures are localized in space, travel at constant velocity without deformation and cross each other without significant change in shape nor in velocity; their velocity depends on their amplitude.

We derived a model which admits two kinds of solutions, namely shock waves and subsonic depression solitary waves. The former were identified to the capillary hydraulic jumps reported in [13]. The latter compare very well to the experimental data from the bubble-burst experiment, in favor of identifying the constrictions observed to solitons.

The present model is unable to predict the value of the dimensionless contraction amplitude a_-, which is found experimentally to be almost constant, close to 0.8. This feature might be explained by dissipative effects that we neglected at the first order. As it is the case for the

capillary hydraulic jumps [15], a selection mechanism for the velocity could arise from the viscous shear. The slight asymmetry of the patterns observed experimentally could also result from some difference in dissipation on the two sides of the constriction in relation to the convergent/divergent nature of the flow.

To conclude, this study emphasizes the role of inertia in the relaxation dynamics of a Plateau border and that this liquid foam microchannel can be used as a quasi-1D model system to study highly non-linear surface waves in fluid dynamics.

VI. ACKNOWLEDGMENTS

We thank Laurent Limat, Thierry Dauxois and Evgeny Ermanyuk for fruitful discussions.

[1] I. Cantat, S. Cohen-Addad, F. Elias, F. Graner, R. Höhler, O. Pitois, F. Rouyer, and A. Saint-Jalmes, Foams: structure and dynamics. Oxford University Press, Oxford, 2013.

[2] H. M. Princen, "Osmotic pressure of foams and highly concentrated emulsions. i. theoretical considerations," Langmuir, vol. 2, p. 519524, 1986.

[3] A. Saint-Jalmes, "Physical chemistry in foam drainage and coarsening," Soft Matter, vol. 2, pp. 836–849, Sept. 2006.

[4] S. Cohen-Addad, R. Höhler, and O. Pitois, "Flow in Foams and Flowing Foams," Annual Review of Fluid Mechanics, vol. 45, no. 1, pp. 241–267, 2013.

[5] D. Desai and R. Kumar, "Flow through a plateau border of cellular foam," Chemical Engineering Science, vol. 37, pp. 1361–1370, Jan. 1982.

[6] K. Koczò and G. Ràcz, "Flow in a plateau border," Colloids and Surfaces, vol. 22, pp. 95–96, Jan. 1987.

[7] M. I. H. Panhuis, S. Hutzler, D. Weaire, and R. Phelan, "New variations on the soap film experiments of Plateau I. Experiments under forced drainage," Philosophical Magazine Part B, vol. 78, pp. 1–12, July 1998.

[8] S. A. Koehler, S. Hilgenfeldt, E. R. Weeks, and H. A. Stone, "Drainage of single Plateau borders: Direct observation of rigid and mobile interfaces," Phys. Rev. E, vol. 66, p. 040601, Oct. 2002.

[9] O. Pitois, C. Fritz, and M. Vignes-Adler, "Hydrodynamic resistance of a single foam channel," Colloids and Surfaces A: Physicochemical and Engineering Aspects, vol. 261, pp. 109–114, July 2005.

[10] K. Piroird and E. Lorenceau, "Capillary Flow of Oil in a Single Foam Microchannel," Phys. Rev. Lett., vol. 111, p. 234503, Dec. 2013.

[11] R. Mensire, K. Piroird, and E. Lorenceau, "Capillary imbibition of aqueous foams by miscible and nonmiscible liquids," Phys. Rev. E, vol. 92, p. 053014, Nov. 2015.

[12] S. A. Koehler, S. Hilgenfeldt, and H. A. Stone, "Liquid Flow through Aqueous Foams: The Node-Dominated Foam Drainage Equation," Phys. Rev. Lett., vol. 82, pp. 4232–4235, May 1999.

[13] A. Cohen, N. Fraysse, J. Rajchenbach, M. Argentina, Y. Bouret, and C. Raufaste, "Inertial mass transport and capillary hydraulic jump in a liquid foam microchannel," Phys. Rev. Lett., vol. 112, p. 218303, 2014.

[14] A. Cohen, N. Fraysse, and C. Raufaste, "Drop coalescence and liquid flow in a single plateau border," Phys. Rev. E, vol. 91, p. 053008, 2015.

[15] M. Argentina, A. Cohen, Y. Bouret, N. Fraysse, and C. Raufaste, "One-dimensional capillary jumps," J. Fluid Mech., vol. 765, p. 116, 2015.

[16] J. S. Russell, "Report on waves. report of the fourteenth meeting of the british association for the advancement of science, york, september 1844," London: John Murray, pp. 311–390, 1845.

[17] M. Remoissenet, Waves called solitons: concepts and experiments. Third edition, Springer-Verlag, Berlin, 1999.

[18] T. Dauxois and M. Peyrard, Physics of solitons. Cambridge University Press, 2006.

[19] E. Falcon, C. Laroche, and S. Fauve, "Observation of depression solitary surface waves on a thin fluid layer," Physical review letters, vol. 89, no. 20, p. 204501, 2002.

[20] S. Perrard, L. Deike, C. Duchne, and C.-T. Pham, "Capillary solitons on a levitated medium," Phys. Rev. E, vol. 92, p. 011002, July 2015.

[21] "See supplemental material at ... for a typical movie of the bubble-burst experiment.,"